LATVIAN JOURNAL OF PHYSICS
AND TECHNICAL SCIENCES
2025, N 4

DOI: 10.2478/lpts-2025-0028

INVESTIGATION OF PERTAMAX (GASOLINE) POOL FIRE IN CONFINED COMPARTMENT

T. Rohman[1]*, S. F. Junjunan[1], M. A. Moelyadi[2]

[1]National Research and Innovation Agency (BRIN),
Jalan Jendral Gatot Subroto 10, Jakarta, 12710, INDONESIA
[2]Bandung Institute of Technology (ITB),
Jl Tamansari no 64, Bandung, 40116, INDONESIA
*e-mail: tauf019@brin.go.id

An understanding of fire is needed as a basis for fire suppression, especially in a compartment. Large fires can cause material losses and loss of life, as well as the release of toxic substances into the environment. These fires can be triggered by fuel leaks that form pool fires. Therefore, the characteristics and behaviour of the fire in the compartment were investigated. Experiments were conducted inside a cube-shaped compartment measuring 1.2 m3 in volume with three square pool pans: 14, 21, and 28 cm. The fuel used was Pertamax, an engine fuel produced by Pertamina and commonly used in Indonesia. The experimental results showed that the size of the fire indicated by the Heat Release Rate (HRR) value was influenced by the cross-sectional area of the pool fire, which would affect the maximum temperature and duration of the flame in the closed compartment. This is related to the heat flux and oxygen consumption rate. Numerical simulations were also carried out using the Fire Dynamics Simulator (FDS version 6.7.9), yielding results that closely matched the experimental results, with differences of less than 20 % for the HRR value. It is expected that by knowing the characteristics and behaviour of the fire, research can be continued on the fire extinguishing system in the compartment.

Keywords: *Confined compartment, fire dynamics, heat release rate (HRR), Pertamax, pool fire, simulator (FDS).*

1. INTRODUCTION

Research on the characteristics of both indoor and outdoor fires has been conducted both analytically and experimentally for a long time. In general, however, analytical models [1] do not capture the complexity of this phenomenon because they often make one or more simplifying assumptions, such as ignoring some forms of displacement or holding flame temperatures and chemical species concentrations constant. One of the analytical approaches is the study by Palazzi et al. on pool fires in hydrocarbons inside semi-enclosed compartments [2], [3].

Many experimental studies have been conducted in the past to achieve realistic solutions. Experimental results show that pool fire is affected by a number of coupled parameters, such as pool geometry, fuel type, ambient conditions, etc. [4]. Some examples of experimental studies were conducted by Soleh et al. using heptane as a fuel source [5]. Then some use methanol, ethanol, and various other fuels as pool fire sources both inside the compartment and outdoors [6]–[8]. Additionally, experimental studies have been conducted to examine the fire characteristics within aircraft cargo compartments [9], [10].

Recent research shows that the use of numerical simulation is becoming a trend in analysing fire characteristics, as Tuovinen simulated hydrocarbon combustion in a ventilated room using CFD [11]. Hyde and Moss modelled CO production in a compartment fire based on a laminar flamelet relation [12]. Currently, many numerical simulation studies are being conducted in conjunction with experiments to obtain valid results [13]–[15].

2. EXPERIMENTAL

The compartment used is cube-shaped with a size of 100 cm x 100 cm x 120 cm and made of stainless steel. There are side and front glass windows for visual recording. On the inside, there is a load cell holder to measure the mass of the reduced fuel. Four type-K thermocouples are mounted vertically with a distance between thermocouples ±10 cm parallel to the pool pan. These thermocouples have a maximum temperature capacity of 1200 °C. Oxygen sensors are mounted on the top side of the compartment. This sensor is used to measure the oxygen concentration in the compartment during the experiment. All sensors are connected to a data logger to store the data. Three square pool pans measuring 14 cm (Pan 14), 21 cm (Pan 21), and 28 cm (Pan 28) were used as fuel containers made of 1 mm-thick stainless steel. The setup of the test equipment is shown in Fig. 1.

The fuel used is Pertamax, which is an engine fuel issued by Pertamina and has an octane level of 92. Pertamax is made from HOMC, RCC gasoline, and polygasoline, utilising a product blending process in a blending pool processing unit. This fuel has a density of 715–770 kg/m^3 (at 15 °C), a vapour pressure of 45–60 kPa, and a boiling point of 215 °C [16].

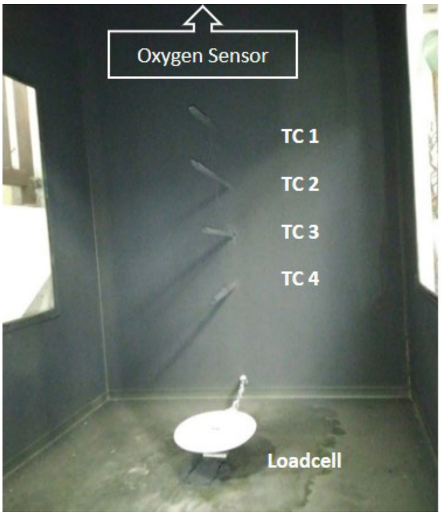

Fig. 1. Schematic and position of sensors inside confined compartment.

3. NUMERICAL SIMULATION

CFD modelling is commonly used in several engineering disciplines to analyse fire dynamics. CFD is used in weather forecasting, aerodynamics, and turbomachinery technology, as well as in closed fire modelling [17]. CFD models are based on time-dependent three-dimensional conservation laws. The simulated domain is divided into many sub-volumes where the laws of momentum, mass and energy conservation are applied to each sub-volume [18].

3.1. Grid Dimension

In the fire scenario, the relationship between the fire characteristic diameter, D*, and the grid cell size, δx, will indicate the accuracy of LES modelling of fluid motion on the sub-grid. The cell dimensions are chosen based on the rule of thumb that the plume resolution, RI, should be greater than or equal to 10, which means that the fire characteristic diameter, D*, should span 10 or more cells [19].

$$RI = \frac{D^*}{\delta x}. \quad (1)$$

$$D^* = \left(\frac{\dot{Q}}{\rho_\infty T_\infty Cp\sqrt{g}}\right)^{2/5}, \quad (2)$$

where $\dot{Q}$ is the total HRR (W) and δx is the grid cell width (m).

3.2. Gas Phase Equations

FDS solves the Navier-Stokes equations at low Mach numbers using Large Eddy Simulation (LES) as the turbulence model. The low Mach number approach defines the pressure as a combination of background pressure $\bar{P}$ and disturbance $\tilde{P}$. The background pressure is given using the ideal gas law:

$$\bar{P} = \frac{\rho R_g T}{W}, \tag{3}$$

where ρ is density (kg·m^{-3}), R_g is the universal gas constant (J·mol^{-1}·K^{-1}), T is temperature (K), and W is molecular weight (kg·mol^{-1}). The momentum equation is expressed as follows:

$$\frac{\partial \boldsymbol{u}}{\partial t} \underbrace{- \boldsymbol{u} \times \omega - \frac{1}{\rho}[(\rho - \rho_\infty) g + \nabla.\tau]}_{\text{Advective}} + \nabla H_p - \underbrace{\tilde{P}\nabla\frac{1}{\rho}}_{\text{Baroclinic}} = 0. \tag{4}$$

$$H_p = \frac{|\boldsymbol{u}^2|}{2} + \frac{\tilde{P}}{\rho}. \tag{5}$$

Default turbulence model in FDS to approximate the viscous stress tensor is the Deardorff turbulence model [20] is used, along with other turbulence models such as the constant coefficient Smagorinsky model [21] and the dynamic Smagorinsky model [22]. The conservation equations for mass, species, and energy are as follows:

$$\frac{\partial \rho}{\partial t} + \nabla.(\rho \boldsymbol{u}) = 0; \tag{6}$$

$$\frac{\partial(\rho y_i)}{\partial t} + \nabla.\rho y_i \boldsymbol{u} = \nabla.(\rho D_g)_i \nabla y_i + \dot{m}'''; \tag{7}$$

$$\frac{\partial(\rho h_s)}{\partial t} + \nabla.(\rho h_s \boldsymbol{u}) = \frac{\partial \bar{P}}{\partial t} + \boldsymbol{u}.\nabla\bar{P} + \dot{Q}''' - \nabla\dot{\boldsymbol{Q}}''; \tag{8}$$

$$\dot{\boldsymbol{Q}}'' = -k\nabla T - \sum_i h_{s,i}\rho D_i \nabla Z_i + \dot{Q}_r''. \tag{9}$$

The conservation equations are solved simultaneously for velocity, temperature, pressure, and mixing fraction at a given time step using an explicit second-order predictor/corrector scheme. The pressure and momentum equations are coupled during the iteration procedure. First the advective and baroclinic parts of the momentum equation are calculated, then the pressure equation is solved several times until the normal components of velocity and background pressure converge to a certain tolerance. The velocity is then recalculated for the next time step. The procedure is iterated until the velocity and pressure converge to a certain tolerance.

4. COMBUSTION MODELLING

The technique used is the mixing fraction of combustion. This technique is based on the assumption that conduction and radiation transfer phenomena occur on a large scale in addition to physical processes that occur on a small scale over time. The chemical model in FDS is the following simple chemical model, which will then be used to calculate the stoichiometric coefficients:

$$C_x H_y O_z N_v + \nu_{O_2} O_2 \rightarrow \nu_{CO_2} CO_2 + \nu_{H_2O} H_2O + \nu_{CO} CO + \nu_s Soot + \nu_{N_2} N_2.$$

The stoichiometric equations used to solve fuel and oxidizer consumption rates are:

$$\frac{\dot{m}_F''}{\nu_F M_F} = \frac{\dot{m}_O''}{\nu_O M_O}. \quad (10)$$

While the mixing fraction equation after including the element of the basic conservation law is:

$$\rho \frac{Dz}{Dt} = \nabla . \rho D \nabla Z. \quad (11)$$

From the above equation, the rate of oxygen consumption per unit mass can be derived again to obtain the rate of oxygen consumption per unit mass at any time, as shown in the equation below.

$$-\dot{m}_O'' = \frac{dY_O}{dZ}\Big|_{Z<Zf} \rho D \nabla Z . \boldsymbol{n}. \quad (12)$$

5. THERMOCOUPLE MODELLING

The FDS thermocouple model is used to compare the temperature field calculated in FDS with the temperature uncorrected experimental data. This allows the simulation to account for the thermocouple's thermal mass and radiant heat loss. The thermocouple temperature (T_{TC}) is found by solving the energy balance around the thermocouple:

$$\rho C_p \frac{dT_{TC}}{dt} = \varepsilon \left(\frac{U}{4} - \sigma T_{TC}^4 \right) + h(T_g - T_{TC}), \quad (13)$$

where ε is the thermocouple emissivity, h is the convection heat transfer coefficient (W·m-2K-1), and T_g is the actual gas temperature (K). Since all thermocouples are type K, the density, heat capacity, and emissivity are set at nickel material with $\rho = 8909\ kg \cdot m^{-3}$ and $Cp = 0.44\ kJ \cdot kg^{-1} \cdot K^{-1}$, and ε = 0.9.

6. GEOMETRY DOMAIN

The geometry domain corresponds to the interior of the compartment, with the position and size of the pan determined by the test scenario. Thermocouples and oxygen sensors are installed at the test positions to view temperature values and oxygen levels. The simulated fuel mass is 100 g for all pan sizes. The simulation parameter data is presented with the simulation domain shown in Fig. 2. The Pertamax property data in Table 1 are the values from the literature case that uses gasoline as the fuel.

Table 1. Properties of Pertamax

CO Yield	0.016 kg/kg
Soot Yield	0.051 kg/kg
Heat of combustion	44700 kJ/kg
Density	723 kg/m^3
Specific heat	2.22 kJ/(kg·K)
Conductivity	0.124 W/(m·K)

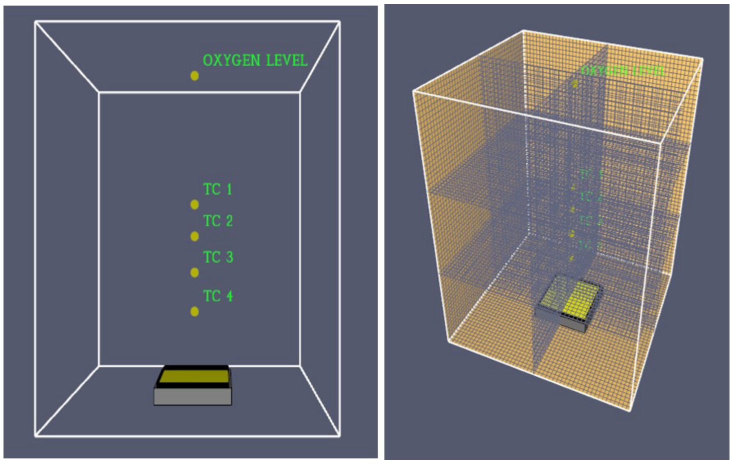

Fig. 2. Simulation domain and setup.

7. RESULTS AND DISCUSSION

Pan 14 has the smallest cross-sectional area, resulting in a small flame size and thus a long flame duration. This is evident in Figure 3, which shows the oxygen level decreasing gradually until it is extinguished at the 9 % concentration level. The long duration of the flame causes the temperature inside the compartment to be the highest compared to the other pan sizes, as seen in Fig. 3. The numerical simulation also shows the same trend as the experimental results.

Pan 21 and Pan 28 have similar characteristics because the combustion mode is optically thin and radiative in contrast to Pan 14, which forms turbulence and is convective. This is in accordance with the definition by Baubraska [1983], which describes the burning mode in pool fire based on the diameter of the pan (in this experiment, approximated by a square diagonal line). The definition is shown in Table 2 [23].

Table 2. Pool Diameter and Burning Mode

Pool diameter (cm)	Burning mode
< 5	Laminar, convective
5–20	Turbulent, convective
20–100	Optically thin, radiative
> 100	Optically thick, radiative

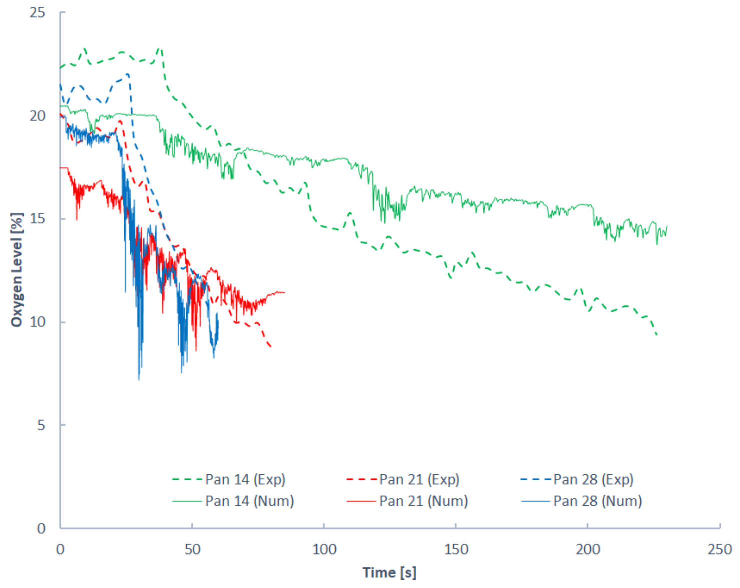

Fig. 3. Concentration of oxygen during fire burning until flames out.

The maximum temperature measured on the thermocouple has a graphical trend that is close between the experiment and the simulation as seen in Fig. 4. There is something different in Pan 14 compared to the other pan, namely, the value of the simulation is lower than that of the experiment. This is related to the longer duration of the flame in the compartment so that the sensitivity of the thermocouple sensor increases. The difference in maximum temperature values in all pans is due to incomplete fuel property values (Pertamax), so it is combined with fuel data from the literature.

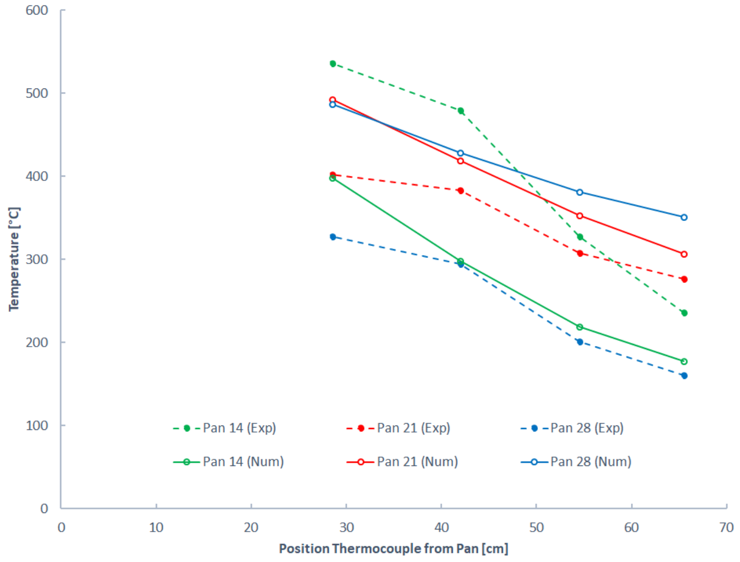

Fig. 4. Maximum temperature at each thermocouple.

A large HRR results in a faster fuel consumption rate so that the oxygen levels in the compartment are quickly depleted and the fire goes out. This is inversely proportional to the maximum temperature value. Due to the short flame duration, the heat flux is also short as shown in Fig. 5.

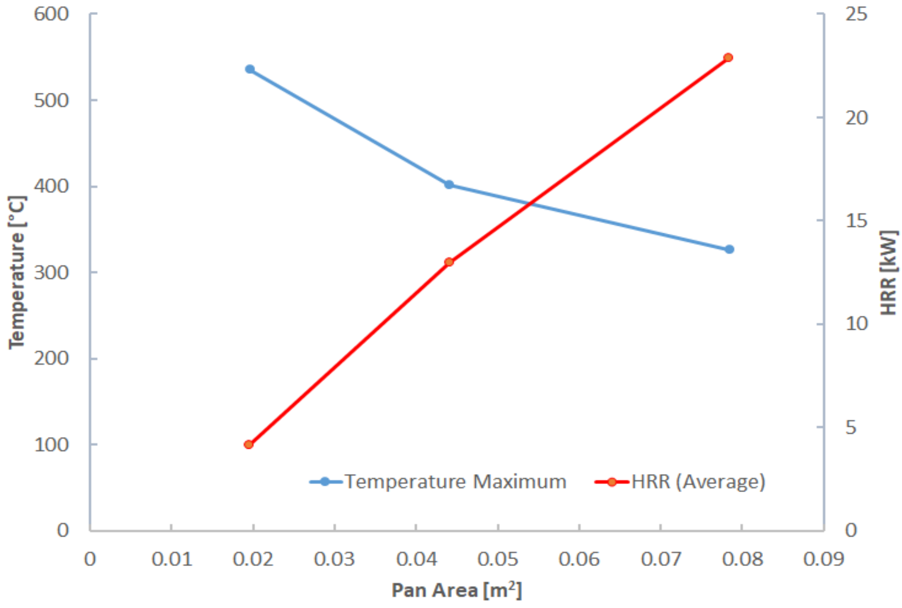

Fig. 5. Effect of pan area to temperature maximum and HRR.

The comparison of experimental results with simulation is presented in Table 3 and Fig. 6. The relatively small percentage difference in HRR indicates that the numerical modelling performed is close to the experimental results. As for the maximum temperature value, the difference is still quite large due to the fuel properties that are not in accordance with those used in experiments.

Table 3. Comparison of Experiment and Simulation

	T_{max} (°C)		HRR Average (kW)		%Δ T_{max}	%Δ HRR
	Exp	Num	Exp	Num		
Pan 14	536	398	4.16	4.05	-25.7	-2.6
Pan 21	402	493	12.97	10.64	22.7	-18.0
Pan 28	327	487	22.85	23.34	48.8	2.1

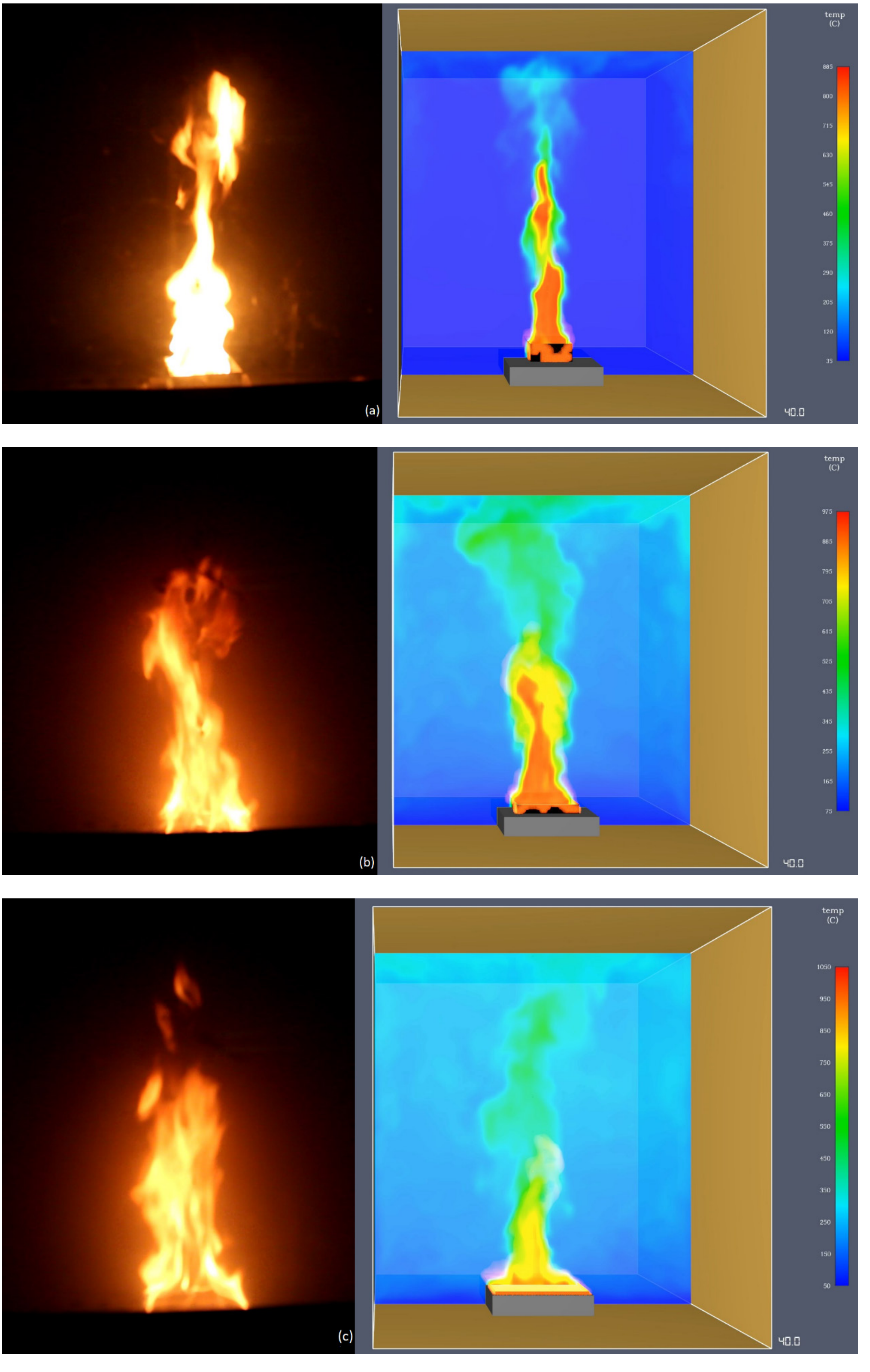

Fig. 6. Comparison simulation and experiment at t=40s (a) Pan 14, (b) Pan 21, and (c) Pan 28.

8. CONCLUSION

The aim of this research has been to obtain data on the behaviour and characteristics of a fire in an enclosed compartment using a computational simulation study and then validate by experimental testing. From the work performed, it has been concluded that the characteristics of a fire in a closed compartment are affected by the cross-sectional area of the pan. The trend is that the HRR value increases as the cross-sectional area of the pan increases. An increase in HRR requires more oxygen, so the oxygen content in the closed compartment decreases rapidly. Therefore, the heat flux lasts for a short time as the flame extinguishes.

Flame size affects the flame shape and the combustion mode. A larger flame indicates a more turbulent flame. Flame size increases the total heat flux and the average temperature in the compartment, even though this occurs at the maximum temperature in the compartment. The increased heat flux and average temperature in the compartment and the depletion of the oxygen concentration lead to more production of unburned gas and vaporized fuel, which causes flashover in the compartment. At the same time, however, the low oxygen level causes the fire in the compartment to self-extinguish. These combustion phenomena can occur simultaneously and interact with each other.

Numerical simulations using FDS are strongly influenced by input parameters, including fuel properties. Differences in values will lead to differences with experimental results. More in-depth studies are needed to improve the accuracy and validation of numerical simulation results so that they can be used as a reference in the design of fire suppression systems in buildings or compartments.

REFERENCES

1. Armendáriz, J., & Matalon, M. (2001). Evaporation and Combustion of Thin Films of Liquid Fuels. *Journal of Fluid Mechanics, 435*, 351–376. https://doi.org/10.1017/S002211200100413X
2. Palazzi, E., & Fabiano, B. (2012). Analytical Modelling of Hydrocarbon Pool Fires: Conservative Evaluation of Flame Temperature and Thermal Power. *Process Safety and Environmental Protection, 90* (2), 121–128. https://doi.org/10.1016/j.psep.2011.06.009
3. Palazzi, E., Caviglione, C., Reverberi, A. P., & Fabiano, B. (2017). A Short-Cut Analytical Model of Hydrocarbon Pool Fire of Different Geometries, with Enhanced View Factor Evaluation. *Process Safety and Environmental Protection, 110*, 89–101. https://doi.org/10.1016/j.psep.2017.08.021
4. Joulain, P. (1998). The Behavior of Pool Fires: State of the Art and New Insights. *Symposium (International) on Combustion, 27* (2), 2691–2706. https://doi.org/10.1016/S0082-0784(98)80125-2
5. Junjunan, S. F., Chetehouna, K., Cablé, A., Abdlgwad, A., Oger, A., & Bura, R. O. (2022). Study of heptane pool fire in well-confined military vehicle engine compartment. In *Proceedings of CONV-22: Int. Symp. on Convective Heat and Mass Transfer.* 5–10 June 2022, Turkey, Begel House Inc. https://doi.org/10.1615/ICHMT.2022.CONV22.200
6. Chan Kim, S., Lee, K. Y., & Hamins, A. (2019). Energy Balance in Medium-Scale Methanol, Ethanol, and Acetone Pool Fires. *Fire Safety Journal, 107,* 44–53. https://doi.org/10.1016/j.firesaf.2019.01.004

7. Sahu, D., Jain, S., Gupta, A., & Kumar, S. (2019). Experimental Studies on Different Liquid Pool Fires inside the Compartment. *Fire Safety Journal, 109,* 102858. https://doi.org/10.1016/j.firesaf.2019.102858
8. Tian, X., Liu, C., Zhong, M., & Shi, C. (2020). Experimental Study and Theoretical Analysis on Influencing Factors of Burning Rate of Methanol Pool Fire. *Fuel, 269,* 117467. https://doi.org/10.1016/j.fuel.2020.117467
9. Pathak, A., Norrefeldt, V., & Pschirer, M. (2021). Validation of a Simulation Tool for an Environmentally Friendly Aircraft Cargo Fire Protection System. *Aerospace, 8* (2), 35. https://doi.org/10.3390/aerospace8020035
10. Tao, Z., Yang, W., Sun, Z., Chen, M., Wang, J., Yang, R., & Zhang, H. (2022). Experimental Study of Oil Pool Shape and Environment Pressure on the Wall Fire Behavior in an Airplane Cargo Compartment. *International Journal of Thermal Sciences, 174,* 107440. https://doi.org/10.1016/j.ijthermalsci.2021.107440
11. Tuovinen, H., & McNamee, M. (2000). *Incorporation of Detailed Chemistry in CFD Modelling of Compartment Fires.* ISFEH, Lake Windermere.
12. Hyde, S. M., & Moss, J. B. (2003). Modelling CO Production in Vitiated Compartment Fires. *Fire Safety Science, 7*, 395–406.
13. Brohez, S., Saladino, D., & Perelli, M. (2022). Experimental and Numerical Study of Heptane Pool Fire. *Chemical Engineering Transactions, 91,* 223–228. https://doi.org/10.3303/CET2291038
14. Kumar, A., Kumar, R., & Ansari, A.A. (2022). Experimental and Numerical Simulation Studies of Liquefied Petroleum Gas Fire in a Full–Scale Compartment. *Process Safety Progress, 41* (1), 195–206. https://doi.org/10.1002/prs.12292
15. Li, J., Beji, T., Brohez, S., & Merci, B. (2021). Experimental and Numerical Study of Pool Fire Dynamics in an Air-Tight Compartment Focusing on Pressure Variation. *Fire Safety Journal, 120*, 103128. https://doi.org/10.1016/j.firesaf.2020.103128
16. Pertamina. (2021). *Product-IFM: Pertamax, Pertamina.* Available at: https://onesolution.pertamina.com/Product/Download?filename=20210806090201atc_Pertamax%20Spesifikasi.pdf
17. Yeoh, G. H., & Yuen, K. K. (2009). *Computational Fluid Dynamics in Fire Engineering: Theory, Modelling and Practice*. Butterworth-Heinemann, 545.
18. Karlsson, B., & Quintiere, J. G. (2022). *Enclosure Fire Dynamics.* (2nd ed.). CRC Press.
19. McGrattan, K. B., McDermott, R. J., Weinschenk, C. G., & Forney, G. (2013). *Fire Dynamics Simulator, Technical Reference Guide.* (6th ed.). NIST.
20. Deardorff, J. W. (1980). Stratocumulus-Capped Mixed Layers Derived from a Three-Dimensional Model. *Boundary-Layer Meteorology, 18* (4), 495–527. https://doi.org/10.1007/BF00119502
21. Smagorinsky, J. (1963). General Circulation Experiments with the Primitive Equations: I. The Basic Experiment. *Monthly Weather Review, 91* (3), 99–164. https://doi.org/10.1175/1520-0493(1963)091<0099:GCEWTP>2.3.CO;2
22. Germano, M., Piomelli, U., Moin, P., & Cabot, W. H. (1991). A Dynamic Subgrid-Scale Eddy Viscosity Model. *Physics of Fluids A: Fluid Dynamics, 3* (7), 1760–1765. https://doi.org/10.1063/1.857955
23. Babrauskas, V. (1983). Estimating Large Pool Fire Burning Rates. *Fire Technology, 19* (4), 251–261. https://doi.org/10.1007/BF02380810